Enhanced Degradation of Ultra-Violet stabilizer Bis(4-hydroxy)benzophenone using Oxone catalyzed by Hexagonal Nanoplate-assembled CoS 3-Dimensional Cluster

Wei-Jie Liu[a], *Hongta Yang*[b], *Young-Kwon Park*[c], *Eilhann Kwon*[d], *Chao-Wei Huang*[e], *Bui Xuan Thanh*[f], *Ta Cong Khiem*[a], *Siming You*[g], *Farshid Ghanbari*[h,*], *and Kun-Yi Andrew Lin*[a,*]

[a]Department of Environmental Engineering & Innovation and Development Center of Sustainable Agriculture, National Chung Hsing University, 250 Kuo-Kuang Road, Taichung, Taiwan

[b]Department of Chemical Engineering, National Chung Hsing University, 250 Kuo-Kuang Road, Taichung, Taiwan

[c]School of Environmental Engineering, University of Seoul, Seoul 02504, Republic of Korea

[d]Department of Environment and Energy, Sejong University, 209 Neungdong-ro, Gunja-dong, Gwangjin-gu, Seoul, Republic of Korea

[e]Department of Chemical and Materials Engineering, National Kaohsiung University of Science and Technology, Kaohsiung, Taiwan

[f]Faculty of Environment and Natural Resources, Ho Chi Minh City University of Technology, VNU-HCM, 268 Ly Thuong Kiet, District 10, Ho Chi Minh City, 700000, Viet Nam

[g]James Watt School of Engineering, University of Glasgow, Glasgow G12 8QQ, UK

[h]Department of Environmental Health Engineering, Abadan Faculty of Medical Sciences, Abadan, Iran

*Corresponding Authors. E-mail addresses: linky@nchu.edu.tw (KYA Lin); ghanbari.env@gmail.com (F. Ghanbari).

Abstract

As UV-light stabilizers, Bis(4-hydroxy)benzophenone (BBP), are extensively consumed to quench radicals from photooxidation, continuous release of BPs into the environment poses serious threats to the ecology in view of their xenohormone toxicities, and BBP shall be eliminated from water to avoid its adverse effect. Since sulfate radical (SR)-based chemical oxidation techniques have been proven as effective procedures for eliminating organic emerging contaminants, this study aims to develop useful SR-based procedures through activating Oxone for degrading BBP in water. In contrast to the conventional Co_3O_4, cobalt sulfide (CoS) is particularly proposed as an alternative heterogeneous catalyst for activating Oxone to degrade BBP because CoS exhibits more reactive redox characteristics. As structures of catalysts predominantly control their catalytic activities, in this study, a unique nanoplate-assembled CoS (NPCS) 3D cluster is fabricated via a convenient one-step process to serve as a promising heterogeneous catalyst for activating Oxone to degrade BBP. With NPCS = 100 mg/L and Oxone = 200 mg/L, 5 mg/L of BBP can be completely eliminated in 60 min. The catalytic activity of NPCS towards Oxone activation also significantly surpasses the reference material, Co_3O_4, to enhance degradation of BBP. E_a of BBP degradation by NPCS-activated Oxone is also determined as a relatively low value of 42.7 kJ/mol. The activation mechanism as well as degradation pathway of BBP degradation by NPCS-activated Oxone was investigated and validated through experimental evidences and density functional theory (DFT) calculation to offer valuable insights into degradation behaviors for developing SR-based processes of BBP degradation using CoS catalysts.

Keywords: cobalt sulfide, peroxymonosulfate, 4,4-Dihydroxybenzophenone, sulfate radical, nanoplate

1. Introduction

As ultraviolet(UV)-light irradiation reaching the surface of the Earth has substantially increased over the past decades [1], sunscreens have been a typical personal care product to guard our skin from harm of UV irradiation because UV-light stabilizers in sunscreens absorb UV-light irradiation. Among various UV stabilizers, hydroxylated benzophenones (HBPs) and similar compounds, such as acetophenone [2], are frequently used as these reagents are low-cost and effective for absorption of UV [3]. Nevertheless, as HBPs have been extensively consumed and released to various water bodies [4], the presence of HBPs has posed serious threats on the ecology because HBPs have been categorized as emerging contaminants due to their xenohormone toxicities [5-10]. As bis(4-hydroxy)benzophenone (BBP) represents one of the most typical HBPs, BBP has been detected in various water bodies [11], and it is crucial to eliminate BBP from water. However, very few studies have been ever reported to eliminate BBP from water. Therefore, the goal of this work attempts to establish effective methods to eliminate BBP from water.

As advanced oxidation processes (AOPs) have been proven as practical methods for quick and effective elimination of organic pollutants from water [12-14], AOPs should be also promising for degrading BBP. Recently, sulfate radical (SR, $SO_4^{\bullet-}$)-based AOPs are increasingly adopted for degrading emerging contaminants [15] because SR has higher oxidation potentials (2.5–3.1 V) with long half-life [16].

In order to gain SR, Oxone reagent has increasingly adopted as a precursor because Oxone is commercially-available, inexpensive, and environmentally benign [17]. Nonetheless, Oxone necessitates “activation” to be quickly decomposed for production of SR. Although Oxone can be activated through a number of procedures, using transition metals, namely cobalt (Co), to catalytically activate Oxone is the most practical procedure [18-21]. Therefore, Co^{2+} ions are frequently used for activating

Oxone; however its homogeneous nature would make Co^{2+} ions difficult for recovery [22-32]. While cobalt oxides (e.g., Co_3O_4) have been then regarded as an alternative to Co^{2+} for activating Oxone, another solid Co-based material, cobalt sulfides (CoS), have also received increasing attention for serving as a heterogeneous catalyst to Co^{2+} to activate Oxone because of CoS exhibits more reactive redox characteristics [33]. Thus, CoS has been validated to successfully and efficiently activate Oxone to degrade emerging contaminants [34].

Nevertheless, studies of using CoS for activating Oxone to degrade BBP are extremely rare. Thus, the aim of this study is to develop and investigate CoS for activating Oxone to degrade BBP. Since structures of heterogeneous catalysts predominantly control their catalytic activities, CoS with hierarchical nanostructures should exhibit higher surface areas, and surficial reactivity for catalytic applications [35-37]. Therefore, this study attempts to develop a special CoS with three dimensional(3D) hierarchical nanostructures to activate Oxone for the first time in degrading BBP. This nanostructured-CoS can be conveniently fabricated via a one-step hydrothermal process to exhibit a morphology of 3D cluster in which many nanoplates (NPs) are assembled and stacked, forming a NP-assembled CoS (NPCS) cluster. With such an advantageous morphology, and high activity of CoS, NPCS should be a useful heterogeneous catalyst for activating Oxone to degrade BBP. Both experimental evaluation and theoretic study of BBP degradation by NPCS-activated Oxone are then conducted to further provide insights into behaviors and mechanisms of BBP degradation.

2. Experimental

For fabricating NPCS via one-step synthesis, a scheme is illustrated in Fig. 1(a). Initially, 15 mmol of $CoCl_2$ and 60 mmol of thiocarbamide were both added into 100

mL of DI water. The resulting mixture was then added to an autoclave, and heated at 180 °C for a 12-hr hydrothermal process. Subsequently, the precipitate was then collected and rinsed thoroughly, and dried at 60 °C to produce NPCS [38]. Characterizations and experimental protocols of BBP degradation can be found in the supporting information.

3. Results and Discussion

3.1 Physical and chemical properties of NPCS

Appearance of the as-synthesized material via the one-step hydrothermal process can be observed in Fig. 1(b), in which many granules with hexagonal shapes can be detected. Sizes of these granules ranged from 2 to 5 μm, and a zoom-in image (Fig. 1(c)) further unveiled that these hexagonal granules consisted of many interwoven plates. Moreover, these plates were quite thin, and the thicknesses was a few tens of nanometers. The TEM image (Fig. 1(d)) also validates that this resulting product possessed the perfect hexagonal shape, and many NPs were interwoven and assembled onto the granule. These results demonstrate that the one-step hydrothermal process of Co, and thiocarbamide could lead to the formation of hexagonal granules with clear edges, and interwoven NPs, forming an interesting 3D-structured cluster.

To further identify the chemical composition of such a 3D-structured cluster, its EDX spectrum was measured and shown in Fig. 2(a), in which strong signals of Co, and S could be found, and no other significant elements can be detected. On the other hand, its XRD pattern is also shown in Fig. 2(b), and noticeable peaks can be observed at 30, 35.3, 46.9, and 54.4°, which corresponded to the (110), (101), and (102), and (110) planes of CoS based on JCPDS card # 65-3418. These features validated that the resulting 3D-structured clustr was CoS, and this simple one-step hydrothermal process can conveniently transform Co, and thiocarbamide to the hexagonal nanoplate-

assembled CoS (NPCS) cluster. The formation of the unique configuration of NPCS can be attributed to a series of steps [38-40]. Firstly, Co^{2+} and S^{2+} from $CoCl_2$ and thiocarbamide, respectively, would react and rapidly nucleate to form very fine particles which are then congregated to create spherical cores. Since a particular reagent, thiocarbamide, was added as it can serve as a dual function reactant for providing S^{2-}, and acting as a structure-directly agent, thiocarbamide has been validated to be selectively adsorbed onto certain facets of cobalt sulfide crystals, promoting the formation of nanoplate-assembled structure [38-40].

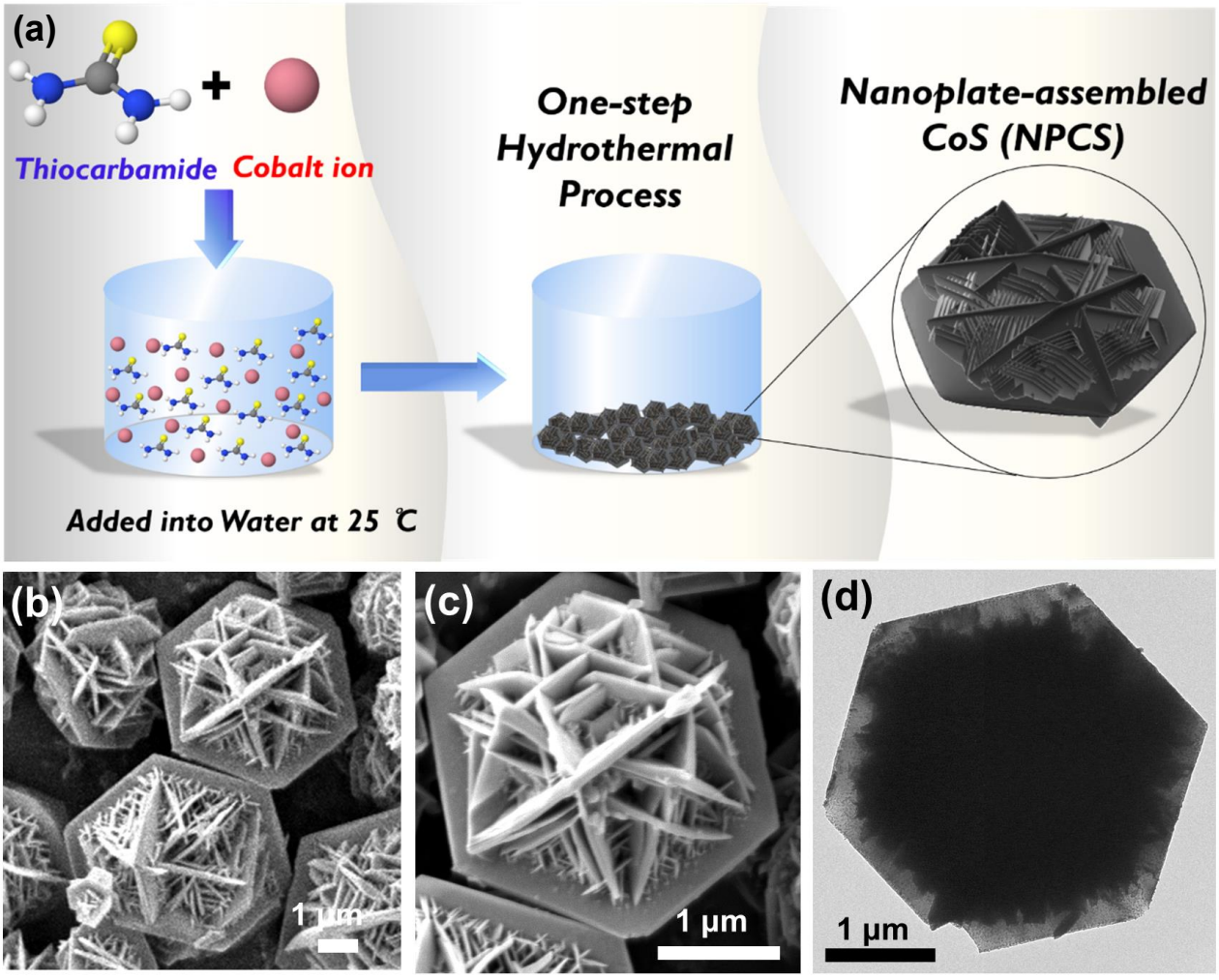

Fig. 1. (a) illustration of preparation scheme for NPCS; (b), (c) SEM images, and (d) TEM image of NPCS.

To further study surface chemistry of NPCS, XPS analysis was employed and displayed in Fig. 2(c). In particular, the Co2p spectrum (Fig. 2(d)) could be then deconvoluted to afford 4 underlying peaks, and the peaks at 781.7 and 797.9 eV could be attributed to Co^{2+} of $Co2p_{3/2}$, and $Co2p_{1/2}$, respectively [35, 41]. Besides, the S2p spectrum could be also deconvoluted to reveal 2 underlying peaks, at 161.7, and 162.9 eV, ascribed to S^{2-} of S2p3/2, and S2p1/2 of CoS, respectively [42], ascertaining the formation of CoS.

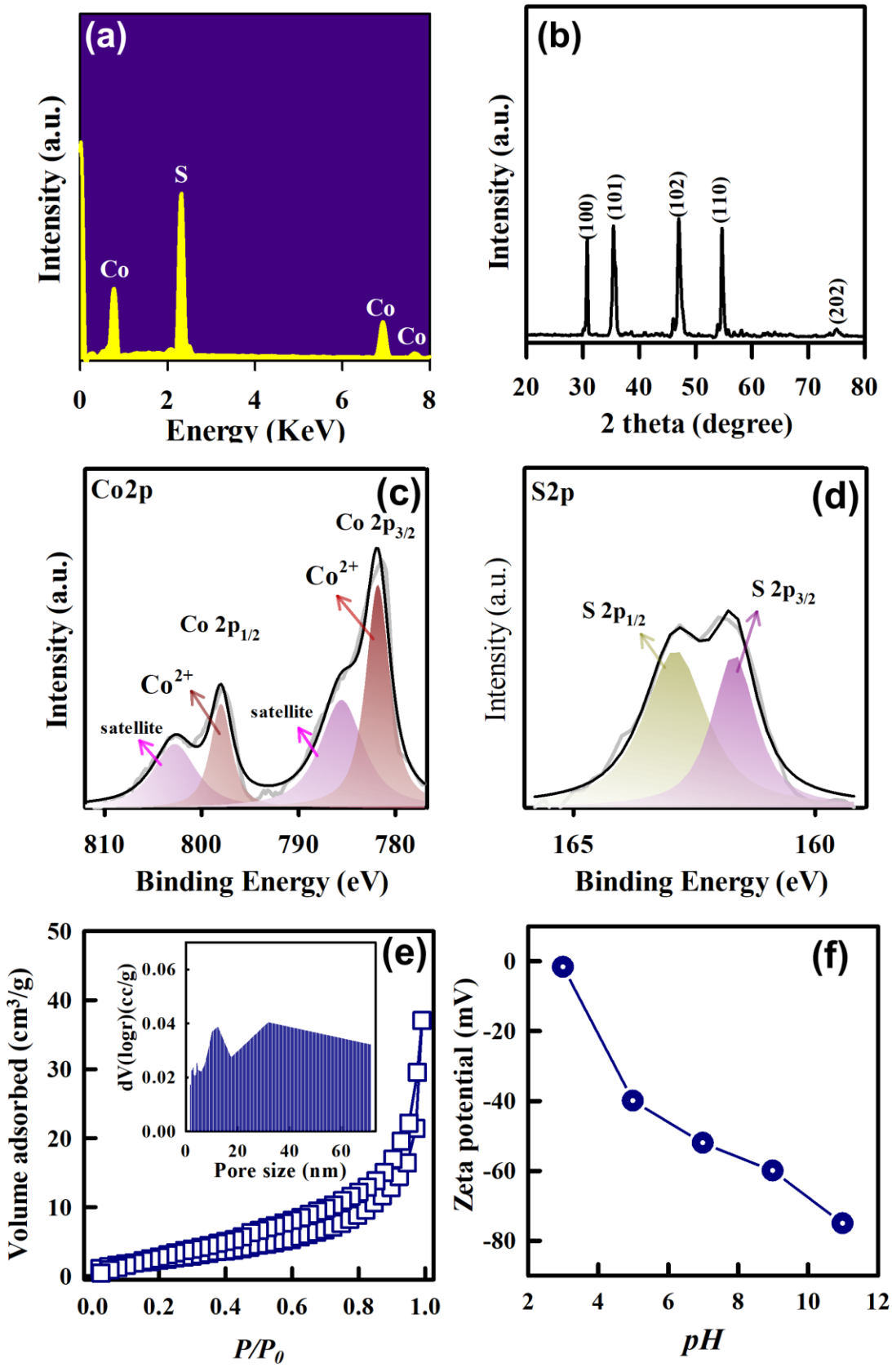

Fig. 2. (a) EDX, and (b) XRD of NPCS; XPS analyses of NPCS: (c) Co2p, and (d) S2p high-resolution spectra; (e) N_2 sorption isotherm (the inset: pore size distribution), and (f) zeta potential of NPCS.

As NPCS possessed this unique NP-assembled 3D cluster, its surficial characteristics were then measured using N_2 sorption isotherms (Fig. 2(e)). The resulting isotherm could be considered as an IUPAC type IV isotherm, suggesting that NPCS shall contain pores, probably derived from spaces between NPs in NPCS. Moreover, a hysteresis loop could be noticed, suggesting the presence of mesopores in NPCS, which could be then validated in the pore size distribution (Fig. 2(e)). The BET surface area of NPCS was then measured as 11 m^2/g and the total pore volume was 0.06 cm^3/g.

Besides, the zeta potentials of NPCS were also measured in Fig. 2(f), and the surface charge of NPCS at pH = 3 was -1.0 mV, which then decreased with the increasing pH values. Specifically, the zeta potential decreased to -40.0 mV at pH = 5, whereas it further decreased to -52.5, -60.0, and -75.5 mV at higher pH = 7, 9 and 11, respectively. This suggested that the surface charge of NPCS appeared to be negative in a typical range of pH values.

3.2 BBP degradation by Oxone activated using NPCS

The as-prepared NPCS was then examined for its catalytic activity for Oxone activation to degrade BBP. Since BBP might be adsorbed to NPCS, leading to adsorptive removal of BBP, it would be critical to verify whether adsorption of BBP to NPCS would occur. As NPCS was added to an BBP solution, the concentration of BBP remained almost the same over 60 min (Fig. 3(a)), revealing that NPCS could not eliminate BBP through adsorption. On the other hand, as Oxone was present without NPCS, the concentration of BBP seemed unchanged in 60 min, demonstrating that Oxone itself without activation was incapable of eliminating BBP at all. Nevertheless, when NPCS and Oxone were both added to the BBP solution, the concentration of BBP gradually decreased over 60 min and its concentration at a certain time t min (C_t) over the initial

concentration (C_0) (i.e., C_t/C_0) reached "0" in 60 min. In view of incompetence of Oxone itself, this result indicated that Oxone was activated by NPCS to generate SR or other derivatives for degrading BBP.

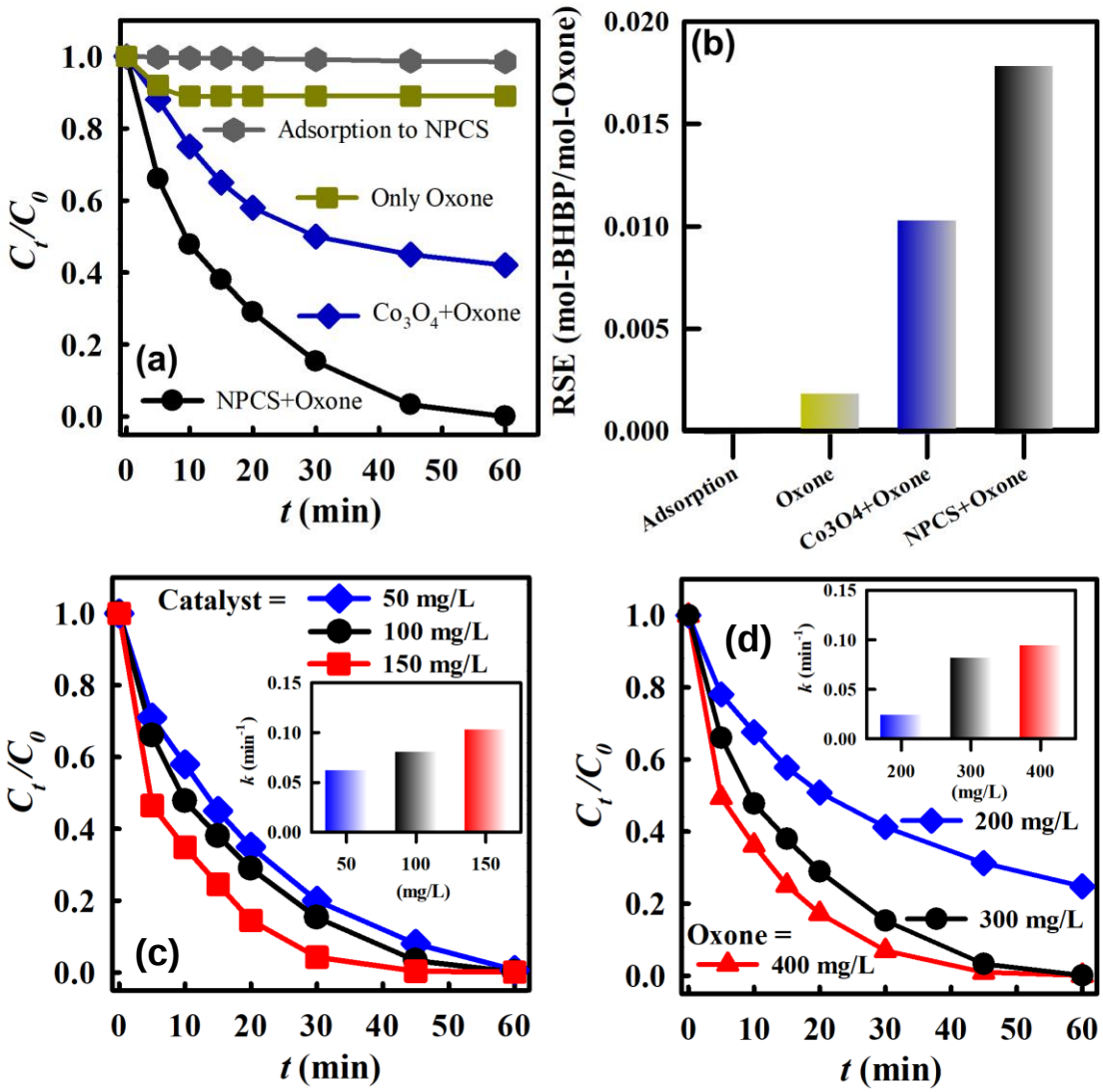

Fig. 3. (a) Degradation of BBP by Oxone, adsorption to NPCS, NPCS+Oxone, and Co_3O_4 NP+Oxone (Catalyst = 100 mg/L, Oxone =200 mg/L, T = 30 ℃); (b) RSE values Degradation of BBP by NPCS+Oxone: (c) effect of NPCS dosage (Oxone =300 mg/L, T = 30 ℃), and (d) effect of Oxone dosage (NPCS = 200 mg/L, T = 30 ℃).

In consideration of Co^{2+} in NPCS, Co^{2+} would react with Oxone to generate SR as follows (Eqs.(1)-(2)) [43, 44]:

$$Co^{2+}@NPCS + HSO_5^- \rightarrow Co^{3+}@NPCS + SO_4^{\bullet-} + OH^- \quad (1)$$

$$Co^{3+}@NPCS + HSO_5^- \rightarrow Co^{2+}@NPCS + SO_5^{\bullet -} + H^+ \quad (2)$$

Moreover, since Co_3O_4 has been deemed as a reference heterogeneous catalyst for Oxone, commercial Co_3O_4 nanoparticles (Fig. S1(a)) were employed for comparison with NPCS for activating Oxone. Fig. 3(a) reveals that Co_3O_4 nanoparticle was also certainly capable of activating Oxone as C_t/C_0 at 60 min reached 0.5. Nevertheless, the degradation efficiency for BBP by Co_3O_4 nanoparticle-activated Oxone was considerably lower than that of NPCS.

To further quantitatively distinguish catalytic activities of NPCS and Co_3O_4 nanoparticle, the corresponding reaction stoichiometric efficiencies (RSE) were then determined as RSE has been increasingly adopted to access catalytic activities of catalysts for activating Oxone to degrade pollutants as follows [45, 46]:

$$\text{Reaction Stoichiometric Efficiency (RSE)} = \frac{\text{BBP degraded (mole)}}{\text{Oxone added (mole)}} \quad (3)$$

The RSE obtained by NPCS, and Co_3O_4 nanoparticle as well as Oxone itself were than displayed in Fig. 3(b). As the amount of Oxone was the same in each case (i.e., 40 mg = 0.26 mmol), NPCS could achieve RSE = 0.018, whereas Co_3O_4 merely reached 0.010, demonstrating that NPCS can utilize Oxone more efficiently to degrade BBP.

While Co_3O_4 nanoparticle has been a benchmark heterogeneous catalyst for Oxone activation, CoS seemed to exhibit more advantageous characteristics than Co_3O_4 nanoparticle. For instance, the cyclic voltammetry (CV) curves of Co_3O_4 and NPCS were both measured, and displayed in Fig. S1(c). In comparison to Co_3O_4 nanoparticle, NPCS showed a much higher current density as well as higher reductive capability to implement redox processes [47]. On the other hand, the linear sweep voltammetry (LSV) of NPCS (Fig. S1(d)) also exhibited the much more increased current than that of Co_3O_4 nanoparticles. These features indicate that NPCS possessed a more superior redox property which would then facilitate its catalytic activity towards Oxone activation.

Even though the commercial Co_3O_4 nanoparticles exhibited very small sizes, these nanoparticles aggregated seriously as displayed in Fig. S1(a), making the commercial Co_3O_4 NP possess a very low surface of 2 m^2/g and pore volume of 0.01 cm^3/g due to its low N_2 sorption (Fig. S1(b)). In contrast, NPCS exhibited the hierarchical structure comprised of NPs, enabling NPCS to show a higher surface area of 11 m^2/g, and a pore volume of 0.06 cm^3/g. Therefore, NPCS can exhibit more reactive surfaces for catalyzing activation of Oxone. These comparisons further validated that the enhanced textural and redox properties of NPCS enabled it to become a more effective catalyst for activating Oxone to degrade BBP.

3.3 Effects of NPCS and Oxone concentrations on BBP degradation

Even though NPCS could activate Oxone for degrading BBP, it would be practical to further examine effects of concentrations of NPCS and Oxone for BBP degradation in Fig.3(c). At first, the concentration of NPCS was set to 50, 100 and 200 mg/L with a fixed Oxone concentration of 200 mg/L. These three concentrations of NPCS all led to the complete elimination of BBP in 60 min, demonstrating that a much lower concentration of NPCS at 50 mg/L could still activate Oxone to fully eliminate BBP.

However, the degradation process seemed much faster at a higher concentration of NPCS. To further quantify the degradation kinetics, the pseudo first order rate law $C_t = C_0 \exp(-kt)$ was then adopted [48], in which k represents the pseudo first order rate constant (min^{-1}) of BBP degradation. As k at NPCS = 50 mg/L was 0.0635 min^{-1} (see the inset), it can noticeably rise up to 0.0818 min-1 at NPCS = 100 mg/L, and then 0.1040 min^{-1} at NPCS = 150 mg/L. The comparison validated that a higher concentration of NPCS considerably enhanced degradation kinetics as more active sites were present in the solution to speed up the reactions.

On the other hand, the effect of Oxone concentration was also changed to 100, 200, and 300 mg/L with a fixed concentration of NPCS of 200 mg/L. Fig.3(d) demonstrates that a relatively low concentration of Oxone as 100 mg/L would lead to incomplete degradation of BBP, and also its corresponding *k* was also relatively low as 0.0241 min^{-1} (as shown in the inset). As the concentration of Oxone increased from 100 to 200, and 300 mg/L, the degradation became much faster with higher *k* of 0.0818, and 0.0944 min^{-1}, respectively. These results ascertained that Oxone concentration was critical and ample Oxone was necessitated to enable full elimination of BBP, whereas a relatively low dosage of NPCS was still useful to activate Oxone to fully eliminate BBP as NPCS served as the role of catalyst.

3.4 Effects of temperature and initial pH on BBP degradation

Fig. 4(a) further reveals BBP degradation by NPCS-activated Oxone at various temperatures. BBP could be all eliminated completely at these temperatures ranging from 30 to 50 °C. BBP degradation also seemed to proceed much faster at higher temperatures. Correspondingly, the *k* value grew considerably at higher temperatures as *k* rose up from 0.0818 at 30 °C to 0.1300 at 40 °C and 0.2345 min^{-1} at 50 °C (see the inset in Fig.4(a)), confirming the positive effect of higher temperatures.

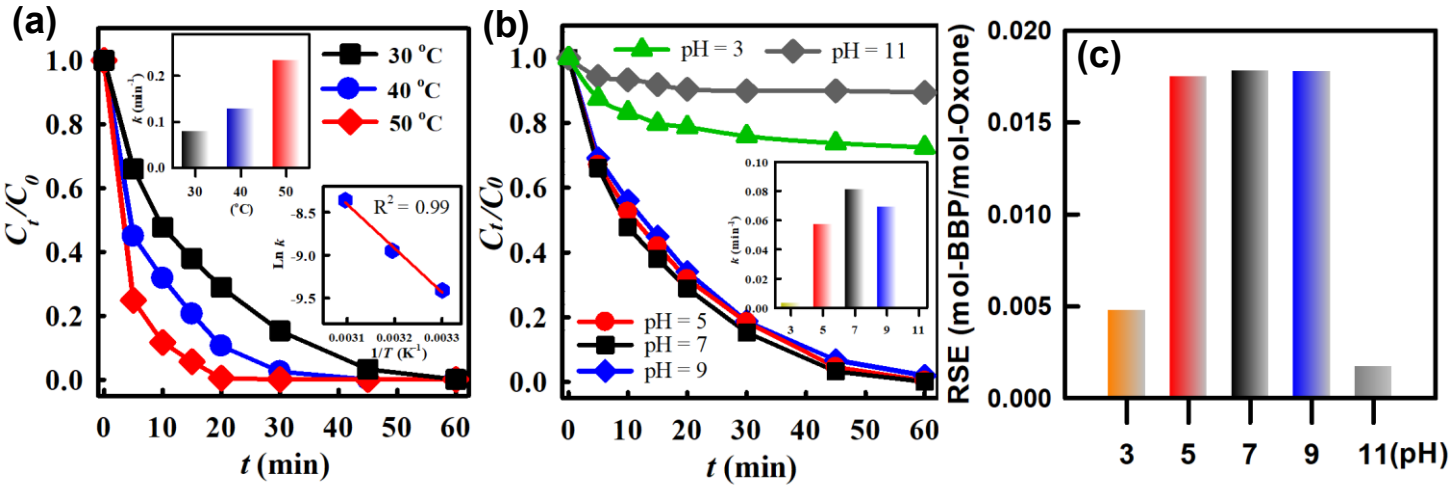

Fig. 4. Degradation of BBP by NPCS+Oxone: (a) effect of temperature (NPCS =100 mg/L; Oxone =200 mg/L), and (b) effect of pH value on degradation kinetics and (c) RSE (NPCS = 100 mg/L; Oxone =200 mg/L; T = 30 °C).

To further analyze the relationship between the kinetics, and temperature, the Arrhenius equation: Ln k = ln A – E_a/RT was further adopted, where E_a represents the activation energy (E_a, kJ/mol) of BBP degradation. The plot of $1/T$ vs. $Ln\ k$ was displayed as the inset in Fig. 4(a) and the data were properly-fitted by the linear regression with R^2 = 0.99 and the calculated E_a was 42.7 kJ/mol, suggesting that the relationship between the kinetics and temperature for BBP degradation by NPCS-activated Oxone would be interpreted by the Arrhenius equation.

On the other hand, because BBP degradation and Oxone activation occur in aqueous solutions, pH shall be an essential parameter, and thus the effect of pH on BBP degradation was then examined. Fig. 4(b) displays that BBP degradation was almost not influenced in weakly acidic and basic environment at pH = 5 and 9 as the corresponding k slightly changed from 0.0818 to 0.0583, and 0.0700 min^{-1}, respectively while BBP could be still completely eliminated in 60 min with unchanged RSE (Fig.

4(c)) under these conditions. This indicates that NPCS exhibited resilience to accommodate slight variation in the solution pH.

On the other hand, when pH was further decreased to pH = 3, degradation of BBP was noticeably affected as *k*, and RSE were considerably decreased because Oxone is prone to remain stable in highly acidic environments, making it less possible to be activated [49]. In the case of BBP degradation at higher pH = 11, BBP degradation was significantly suppressed, as the corresponding RSE became merely 0.002 with an insignificant *k*. A number of previous studies have indicated that Oxone would be prone to self-decomposition without generation of SR under highly alkaline conditions [49, 50]. Therefore, the amount of SR might be insufficient for degrading BBP under the alkaline conditions. On the other hand, the higher pH would also cause the surface of NPCS to be much more negatively-charged because of deposition of hydroxyl ions on the catalyst surface as seen in the zeta potentials (Fig.2(e)), increasing the electrostatic repulsion to refrain contact between $SO_5^{\bullet-}$ and NPCS .

3.5 Effect of water sources, and the recyclability of NPCS

Moreover, as UV-light stabilizer might be present in different types of water, Fig. 5(a) further examines the effect of water types on BBP degradation by NPCS-activated Oxone. As BBP is a common UV stabilizer and contained in many sunscreens, BBP might be released to various water bodies, including ocean, lake, etc. Therefore, it would be useful to examine whether the proposed technique would be applied for removing BBP from seawater. In the case of seawater which contains Na^+, Cl^-, and other anions, BBP could be still degraded effectively even though the kinetics, and RSE

were both slightly affected. On the other hand, BBP in tape water which typically contains chlorine was also tested, and BBP could be fully eliminated in 60 min while the kinetics was also slightly influenced. These results suggest that even though co-existing compounds in water might slightly interfere BBP degradation and Oxone activation, NPCS remained quite effective to activate Oxone to degrade BBP.

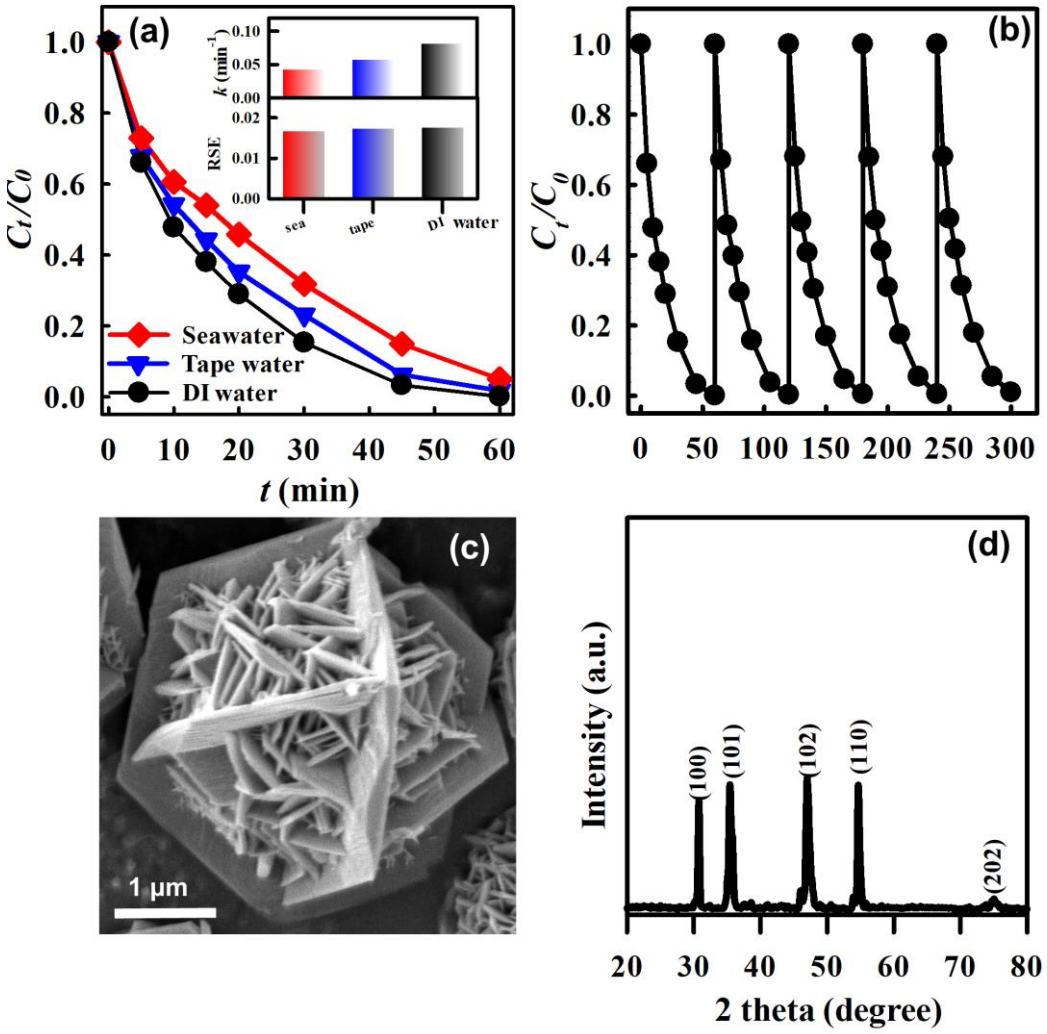

Fig. 5. (a) effects of water sources; (b) recyclability test of NPCS for degradation of BBP (NPCS =100 mg/L; Oxone =200 mg/L; T = 30 °C); (c) SEM, and (d) XRD pattern of the spent NPCS.

On the other hand, as NPCS was proposed as a heterogeneous catalyst, NPCS shall be reusable, and then its recyclability was then examined. Fig. 5(b) reveals BBP

degradation using the used NPCS for 5 cycles, and BBP could be quickly and completely eliminated in each cycle. This indicates that the used NPCS was very stable, and remained catalytically active. Fig. 5(c-d) further displays the SEM image, and XRD pattern of the used NPCS, which were comparable to those of the fresh NPCS. These results validated that NPCS was a reusable, and durable heterogeneous catalyst for activating Oxone to degrade BBP.

3.6 A proposed mechanism of BBP degradation by NPCS-activated Oxone

While NPCS-activated Oxone successfully and efficiently eliminate BBP, it would be essential to further elucidate the degradation mechanism. Although activation of Oxone typically produces SR ($SO_4^{\bullet-}$), SR would also lead to other derivative reactive oxygen species (ROS). For instance, SR reacts with H2O would generate $^{\bullet}OH$ through $SO_4^{\bullet-} + H_2O \rightarrow SO_4^{2-} + {}^{\bullet}OH + H^+$ [51]; thus $^{\bullet}OH$ might also occur and contribute to BBP degradation. On the other hand, non-radical-type ROS, such as, $^1O_2$, is also increasingly reported to be derived from Oxone [52-54]. Therefore, it was important to investigate degradation mechanism of BBP by NPCS-activated Oxone. To this end, effects of ROS inhibitors were then examined by using various reagents, namely, tert-butyl alcohol (BuOH), methanol (MeOH), and NaN_4 for determining their inhibiting effect on $^{\bullet}OH$, $SO_4^{\bullet-}$, and $^1O_2$, respectively.

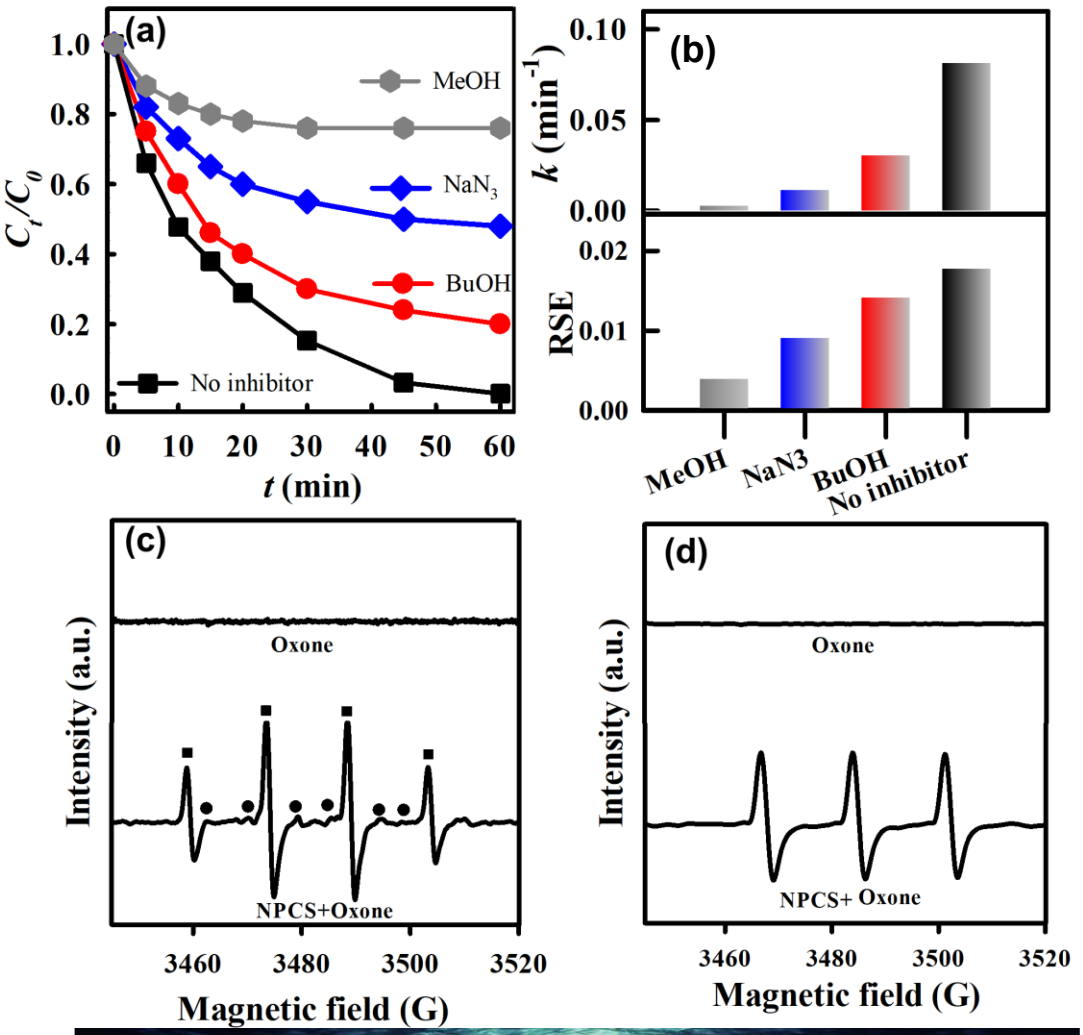

Fig .6. Effects of radical inhibitors on BBP (a) degradation kinetics, and (b) RSE (NPCS = 100 mg/L; Oxone =200 mg/L; T = 30 ℃); EPR analysis using (b) DMPO ((■: DMPO-OH; ●: DMPO- SO_4), and (d) TEMP; (e). a scheme for illustrating the potential mechanism of BBP degradation by NPCS-activated Oxone.

When BuOH was adopted, BBP degradation was slightly influenced as *k* decreased from 0.0818 to 0.0312 min^{-1} (Fig. 6(a-b)), and the corresponding RSE decreased from 0.0180 to 0.0144, implying that $^{\bullet}OH$ might exist, derived from SR. However, $^{\bullet}OH$ seemed not the primary ROS contributing to BBP degradation as the inhibition by BuOH was not significant. Next, when MeOH was then used, BBP degradation was significantly suppressed as *k* and RSE became very low to 0.0037 min-1, and 0.0043, respectively, indicating that SR was present and derived from NPCS-activated Oxone, serving an important ROS for BBP degradation. In addition, when NaN3 was adopted, the corresponding *k* and RSE were also considerably reduced, suggesting that $^{1}O_2$ shall be also present to contributed to BBP degradation.

To further identify ROS derived from NPCS+MPS, Electron spin resonance (ESR) analysis was then employed as displayed in Fig. 6(c). Firstly, as 5,5-Dimethyl-1-Pyrroline-N-Oxide (DMPO) was employed as a spin-trapping agent, no distinct signal was detected in the system of DMPO and Oxone alone. However, while Oxone and NPCS were both present, a perceptible pattern could be noted, ascribed to the hyperfine splitting of oxidation adduct products of DMPO-SO_4, and DMPO-OH [55-57]. Furthermore, when 2,2,6,6-Tetramethylpiperidine (TEMP) was then adopted as a spin-trapping agent in Fig. 6(d), and a distinct pattern of the triplet signal was obtained and corresponding to 2,2,6,6-Tetramethylpiperidinyloxy (TEMPO), validating that the presence of $^{1}O_2$[58]. These results also ascertained that BBP degradation by NPCS-activated Oxone could be attributed to several ROS, such as SR, $^{\bullet}OH$, and $^{1}O_2$ as illustrated schematically in Fig. 6(e).

3.7 DFT calculation, and a potential degradation route for BBP

To further investigate the possible degradation route of BBP by NPCS-activated Oxone, density functional theory (DFT) calculation was adopted for probing into attack of ROS on BBP. The details of DFT calculation can be found in the supporting information, and the optimized structure of BBP is displayed in Fig. 7(a) with its HOMO, and LUMO orbitals visualized in Fig. 7(c). As the green-colored, and red-colored zones indicated electron-poor, and electron-rich zones of BBP. In particular, the HOMO resided on the benzene ring tends to release electrons; therefore, BBP would be attacked by electrophilic ROS, namely, SR, and •OH. Fig. 7(b) summarizes Fukui indices of various reaction sites of BBP. In general, a site with a higher value of Fukui index signifies that this particular site would be more easily attacked. While the site of 3O exhibits the highest value of Fukui index than any other sites, the site of 3O is a saturated site, making it unlikely accept radical addition. In contrast, the site of 5C also shows a significantly higher Fukui index than other sites, making it the most possible site for radical attack. Thus, BBP degradation would be possibly induced by the breakage of the bond between ketone group and benzene ring. Besides, the electrostatic potential distribution of BBP (Fig. 7(d)) also implies the region around 5C would attract the anionic SR, leading to the radical attack.

(a)

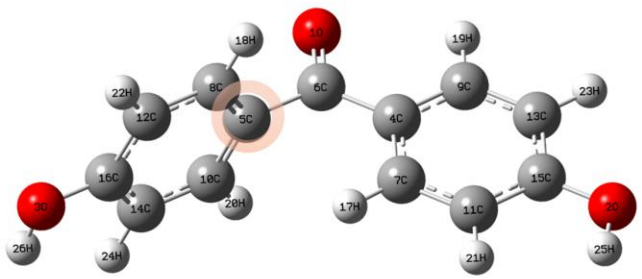

(b)

#Atom		Charge (-1) (e/Å3)	Charge (0) (e/Å3)	Charge (+1) (e/Å3)	f^-
1	O	-0.6892	-0.5459	-0.3775	0.1684
2	O	-0.7251	-0.6816	-0.6252	0.0563
3	O	-0.7123	-0.6910	-0.5972	0.0938
4	C	-0.1951	-0.1869	-0.1638	0.0231
5	C	-0.0939	-0.1496	-0.0670	0.0827
6	C	0.3651	0.5532	0.5522	-0.0010
7	C	-0.2275	-0.1789	-0.1720	0.0069
8	C	-0.2186	-0.2079	-0.1970	0.0109
9	C	-0.2531	-0.1592	-0.1503	0.0089
10	C	-0.2192	-0.2078	-0.1833	0.0246
11	C	-0.3434	-0.3181	-0.2875	0.0306
12	C	-0.3095	-0.2800	-0.2186	0.0614
13	C	-0.2976	-0.2905	-0.2575	0.0330
14	C	-0.3336	-0.3050	-0.2677	0.0373
15	C	0.2357	0.3473	0.3908	0.0436
16	C	0.2966	0.3210	0.3895	0.0686

(c)

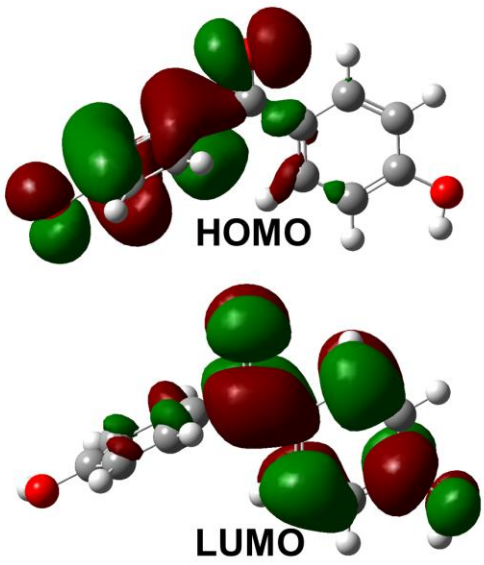

(d)

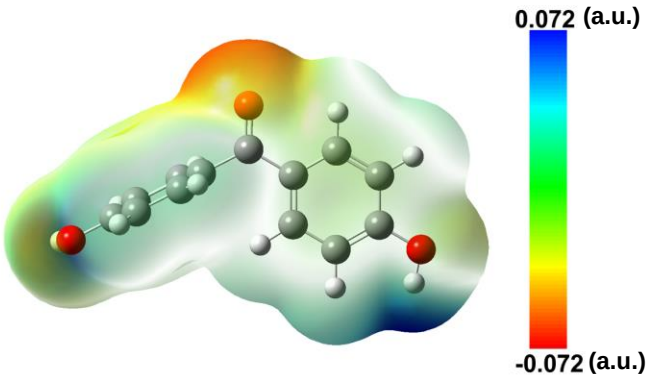

(e)

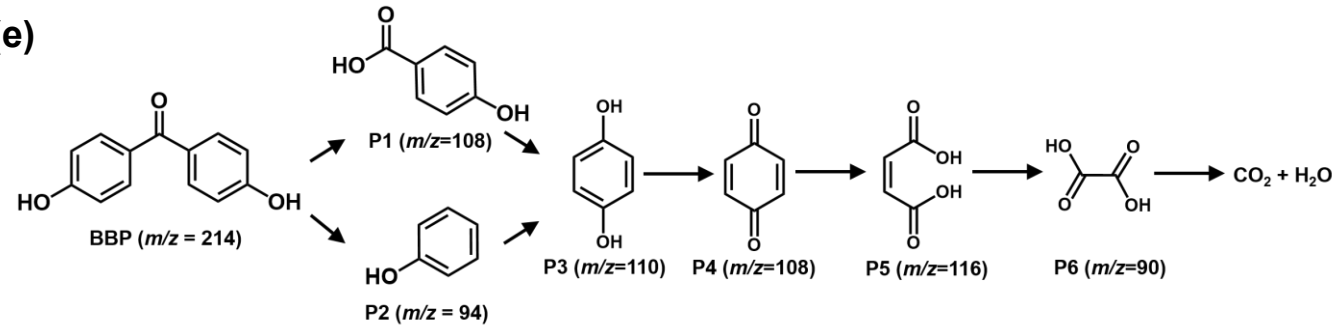

Fig. 7. Natural bond orbital analysis for the BBP molecule at B3LYP/6-31+G(d) level. (a) BBP molecule structure; (b) Natural population analysis (NPA) charge populations and condensed Fukui index distribution for electrophilic attack ($f-$); (c) The highest occupied molecular orbital (HOMO) and the lowest unoccupied molecular orbital (LUMO); (d) Electrostatic potential (ESP)-mapped molecular surface of BBP; (e) A potential degradation pathway of BBP degradation by NPCS+Oxone.

To further identify the degradation route of BBP by NPCS-activated Oxone, degradation intermediates were then analyzed by mass spectrometry, and summarized in Table S1. In view of these intermediates, a potential degradation route of BBP was conceived as Fig. 7(e). As discussed earlier, BBP degradation was initiated by the cleavage of the bond between ketone group and benzene ring to produce two intermediates, P1 (4-hydroxybenzoic acid), and P2 (phenol). Both P1, and P2 would be further oxidized to become P3 (hydroquinone). Subsequently, P3 would be then attacked and underwent a ring-opening reaction to afford P5 (maleic acid), which could be then degraded to result in smaller molecules, including P6 (oxalic acid). Via further oxidation, these smaller molecules would be then broken down into CO_2 and H_2O eventually.

4. Conclusions

In this study, a unique nanoplate-assembled CoS (NPCS) 3D cluster was fabricated via a convenient one-step process to serve as an interesting and promising heterogeneous catalyst for activating Oxone to degrade BBP. With NPCS = 100 mg/L and Oxone = 200 mg/L, 5 mg/L of BBP can be completely eliminated in 60 min, affording a RSE of 0.018. The catalytic activity of NPCS towards Oxone activation also significantly surpassed the reference material, Co_3O_4, to enhance degradation of BBP. E_a of BBP degradation by NPCS-activated Oxone was also determined as a relatively low value of 42.7 kJ/mol. The activation mechanism as well as degradation pathway of BBP degradation by NPCS-activated Oxone was investigated and validated through experimental evidences and DFT calculation to offer insights for developing SR-based processes of BBP degradation using CoS catalysts.

References:

[1] J.R. Herman, Global increase in UV irradiance during the past 30 years (1979–2008) estimated from satellite data, Journal of Geophysical Research: Atmospheres, 115 (2010).

[2] Y. Yu, F. Huang, Y. He, X. Liu, Y. Xu, Y. Zhang, Surface modification of sludge-derived carbon by phosphoric acid as new electrocatalyst for degradation of acetophenone, Environmental science and pollution research international, 25 (2018) 25496-25503.

[3] I. Tarazona, A. Chisvert, Z. León, A. Salvador, Determination of hydroxylated benzophenone UV filters in sea water samples by dispersive liquid–liquid microextraction followed by gas chromatography–mass spectrometry, Journal of Chromatography A, 1217 (2010) 4771-4778.

[4] M.E. Balmer, H.-R. Buser, M.D. Müller, T. Poiger, Occurrence of Some Organic UV Filters in Wastewater, in Surface Waters, and in Fish from Swiss Lakes, Environmental Science & Technology, 39 (2005) 953-962.

[5] N.R. Janjua, B. Mogensen, A.-M. Andersson, J.H. Petersen, M. Henriksen, N.E. Skakkebæk, H.C. Wulf, Systemic Absorption of the Sunscreens Benzophenone-3, Octyl-Methoxycinnamate, and 3-(4-Methyl-Benzylidene) Camphor After Whole-Body Topical Application and Reproductive Hormone Levels in Humans, Journal of Investigative Dermatology, 123 (2004) 57-61.

[6] M.B. Ahmed, M.A.H. Johir, J.L. Zhou, H.H. Ngo, W. Guo, K. Sornalingam, Photolytic and photocatalytic degradation of organic UV filters in contaminated water, Current Opinion in Green and Sustainable Chemistry, 6 (2017) 85-92.

[7] H. Tinwell, P.A. Lefevre, G.J. Moffat, A. Burns, J. Odum, T.D. Spurway, G. Orphanides, J. Ashby, Confirmation of uterotrophic activity of 3-(4-methylbenzylidine)camphor in the immature rat, Environmental Health Perspectives, 110 (2002) 533-536.

[8] C. Schmutzler, I. Hamann, P.J. Hofmann, G. Kovacs, L. Stemmler, B. Mentrup, L. Schomburg, P. Ambrugger, A. Grüters, D. Seidlova-Wuttke, H. Jarry, W. Wuttke, J. Köhrle, Endocrine active compounds affect thyrotropin and thyroid hormone levels in serum as well as endpoints of thyroid hormone action in liver, heart and kidney, Toxicology, 205 (2004) 95-102.

[9] Y.-M. Lee, G. Lee, M.-K. Kim, K.-D. Zoh, Kinetics and degradation mechanism of Benzophenone-3 in chlorination and UV/chlorination reactions, Chemical Engineering Journal, 393 (2020) 124780.

[10] L. Soto-Vázquez, F. Rolón-Delgado, K. Rivera, M.C. Cotto, J. Ducongé, C. Morant, S. Pinilla, F.M. Márquez-Linares, Catalytic use of TiO₂

nanowires in the photodegradation of Benzophenone-4 as an active ingredient in sunscreens, J Environ Manage, 247 (2019) 822-828.
[11] X. Zheng, X.-M. Ren, L. Zhao, L.-H. Guo, Binding and activation of estrogen related receptor γ as possible molecular initiating events of hydroxylated benzophenones endocrine disruption toxicity, Environmental Pollution, 263 (2020) 114656.
[12] J.A. Khan, M. Sayed, S. Khan, N.S. Shah, D.D. Dionysiou, G. Boczkaj, Chapter 9 - Advanced oxidation processes for the treatment of contaminants of emerging concern, in: A.J. Hernández-Maldonado, L. Blaney (Eds.) Contaminants of Emerging Concern in Water and Wastewater, Butterworth-Heinemann, 2020, pp. 299-365.
[13] Q. Chen, X. Zhang, S. Li, J. Tan, C. Xu, Y. Huang, MOF-derived Co3O4@Co-Fe oxide double-shelled nanocages as multi-functional specific peroxidase-like nanozyme catalysts for chemo/biosensing and dye degradation, Chemical Engineering Journal, 395 (2020) 125130.
[14] S. Li, Y. Hou, Q. Chen, X. Zhang, H. Cao, Y. Huang, Promoting Active Sites in MOF-Derived Homobimetallic Hollow Nanocages as a High-Performance Multifunctional Nanozyme Catalyst for Biosensing and Organic Pollutant Degradation, ACS Applied Materials & Interfaces, 12 (2020) 2581-2590.
[15] S.A. Fast, V.G. Gude, D.D. Truax, J. Martin, B.S. Magbanua, A Critical Evaluation of Advanced Oxidation Processes for Emerging Contaminants Removal, Environmental Processes, 4 (2017) 283-302.
[16] T. Olmez-Hanci, I. Arslan-Alaton, Comparison of sulfate and hydroxyl radical based advanced oxidation of phenol, Chemical Engineering Journal, 224 (2013) 10-16.
[17] P. Hu, M. Long, Cobalt-catalyzed sulfate radical-based advanced oxidation: A review on heterogeneous catalysts and applications, Applied Catalysis B: Environmental, 181 (2016) 103-117.
[18] G.P. Anipsitakis, E. Stathatos, D.D. Dionysiou, Heterogeneous Activation of Oxone Using Co3O4, The Journal of Physical Chemistry B, 109 (2005) 13052-13055.
[19] G. Wei, X. Liang, Z. He, Y. Liao, Z. Xie, P. Liu, S. Ji, H. He, D. Li, J. Zhang, Heterogeneous activation of Oxone by substituted magnetites Fe3−xMxO4 (Cr, Mn, Co, Ni) for degradation of Acid Orange II at neutral pH, Journal of Molecular Catalysis A: Chemical, 398 (2015) 86-94.
[20] Z. Li, Z. Chen, Y. Xiang, L. Ling, J. Fang, C. Shang, D.D. Dionysiou, Bromate formation in bromide-containing water through the cobalt-mediated activation of peroxymonosulfate, Water Research, 83 (2015) 132-140.
[21] Q. Chen, X. Zhang, S. Li, J. Tan, C. Xu, Y. Huang, MOF-derived Co3O4@Co-Fe oxide double-shelled nanocages as multi-functional specific peroxidase-like

nanozyme catalysts for chemo/biosensing and dye degradation, Chemical Engineering Journal, 395 (2020).
[22] Q. Yang, H. Choi, S.R. Al-Abed, D.D. Dionysiou, Iron–cobalt mixed oxide nanocatalysts: Heterogeneous peroxymonosulfate activation, cobalt leaching, and ferromagnetic properties for environmental applications, Applied Catalysis B: Environmental, 88 (2009) 462-469.
[23] C. Cai, H. Zhang, X. Zhong, L. Hou, Ultrasound enhanced heterogeneous activation of peroxymonosulfate by a bimetallic Fe–Co/SBA-15 catalyst for the degradation of Orange II in water, J Hazard Mater, 283 (2015) 70-79.
[24] H.-K. Lai, Y.-Z. Chou, M.-H. Lee, K.-Y.A. Lin, Coordination polymer-derived cobalt nanoparticle-embedded carbon nanocomposite as a magnetic multi-functional catalyst for energy generation and biomass conversion, Chemical Engineering Journal, 332 (2018) 717-726.
[25] M.-C. Li, S. Tong, J.-T. Lin, K.-Y.A. Lin, Y.-F. Lin, Electrospun Co3O4 nanofiber as an efficient heterogeneous catalyst for activating peroxymonosulfate in water, J Taiwan Inst Chem Eng, 106 (2020) 110-117.
[26] K.-Y.A. Lin, H.-A. Chang, R.-C. Chen, MOF-derived magnetic carbonaceous nanocomposite as a heterogeneous catalyst to activate oxone for decolorization of Rhodamine B in water, Chemosphere, 130 (2015) 66-72.
[27] K.-Y.A. Lin, F.-K. Hsu, W.-D. Lee, Magnetic cobalt-graphene nanocomposite derived from self-assembly of MOFs with graphene oxide as an activator for peroxymonosulfate, Journal of Materials Chemistry A, 3 (2015) 9480-9490.
[28] K.-Y.A. Lin, J.-T. Lin, X.-Y. Lu, C. Hung, Y.-F. Lin, Electrospun magnetic cobalt-embedded carbon nanofiber as a heterogeneous catalyst for activation of oxone for degradation of Amaranth dye, Journal of Colloid and Interface Science, 505 (2017) 728-735.
[29] K.-Y.A. Lin, T.-Y. Lin, Degradation of Acid Azo Dyes Using Oxone Activated by Cobalt Titanate Perovskite, Water, Air, & Soil Pollution, 229:10 (2018).
[30] K.-Y.A. Lin, M.-T. Yang, J.-T. Lin, Y. Du, Cobalt ferrite nanoparticles supported on electrospun carbon fiber as a magnetic heterogeneous catalyst for activating peroxymonosulfate, Chemosphere, 208 (2018) 502-511.
[31] D.D. Tuan, W.D. Oh, F. Ghanbari, G. Lisak, S. Tong, K.-Y. Andrew Lin, Coordination polymer-derived cobalt-embedded and N/S-doped carbon nanosheet with a hexagonal core-shell nanostructure as an efficient catalyst for activation of oxone in water, J Colloid Interface Sci, 579 (2020) 109-118.
[32] W.-C. Yun, K.-Y.A. Lin, W.-C. Tong, Y.-F. Lin, Y. Du, Enhanced degradation of paracetamol in water using sulfate radical-based advanced oxidation processes catalyzed by 3-dimensional Co3O4 nanoflower, Chemical Engineering Journal, 373 (2019) 1329-1337.

[33] Y. Sun, C. Liu, D.C. Grauer, J. Yano, J.R. Long, P. Yang, C.J. Chang, Electrodeposited Cobalt-Sulfide Catalyst for Electrochemical and Photoelectrochemical Hydrogen Generation from Water, J Am Chem Soc, 135 (2013) 17699-17702.
[34] W. Li, S. Li, Y. Tang, X. Yang, W. Zhang, X. Zhang, H. Chai, Y. Huang, Highly efficient activation of peroxymonosulfate by cobalt sulfide hollow nanospheres for fast ciprofloxacin degradation, Journal of Hazardous Materials, 389 (2020) 121856.
[35] C. Wang, P. Shi, X. Cai, Q. Xu, X. Zhou, X. Zhou, D. Yang, J. Fan, Y. Min, H. Ge, W. Yao, Synergistic Effect of Co3O4 Nanoparticles and Graphene as Catalysts for Peroxymonosulfate-Based Orange II Degradation with High Oxidant Utilization Efficiency, J Phys Chem C, 120 (2016) 336-344.
[36] L. Sun, Y. Bai, K. Sun, Organic molecule controlled synthesis of three-dimensional rhododendron-like cobalt sulfide hierarchitectures as counter electrodes for dye-sensitized solar cells, RSC Advances, 4 (2014) 42087-42091.
[37] J. Zhu, L. Xiang, D. Xi, Y. Zhou, J. Yang, One-step hydrothermal synthesis of flower-like CoS hierarchitectures for application in supercapacitors, Bulletin of Materials Science, 41 (2018) 54.
[38] W. Lin, Y. Huang, G. He, Unique CoS hierarchitectures for high-performance lithium ion batteries, CrystEngComm, 20 (2018) 6727-6732.
[39] M. Zheng, Y. Ding, L. Yu, X. Du, Y. Zhao, In Situ Grown Pristine Cobalt Sulfide as Bifunctional Photocatalyst for Hydrogen and Oxygen Evolution, Advanced Functional Materials, 27 (2017) 1605846.
[40] Q. Wang, L. Jiao, H. Du, W. Peng, Y. Han, D. Song, Y. Si, Y. Wang, H. Yuan, Novel flower-like CoS hierarchitectures: one-pot synthesis and electrochemical properties, Journal of Materials Chemistry, 21 (2011) 327-329.
[41] C. Dong, L. Guo, H. Li, B. Zhang, X. Gao, F. Tian, Y. Qian, D. Wang, L. Xu, Rational fabrication of CoS2/Co4S3@N-doped carbon microspheres as excellent cycling performance anode for half/full sodium ion batteries, Energy Storage Materials, 25 (2020) 679-686.
[42] S. Das, P. Sudhagar, S. Nagarajan, E. Ito, S.Y. Lee, Y.S. Kang, W. Choi, Synthesis of graphene-CoS electro-catalytic electrodes for dye sensitized solar cells, Carbon, 50 (2012) 4815-4821.
[43] S. Muhammad, E. Saputra, H. Sun, J.d.C. Izidoro, D.A. Fungaro, H.M. Ang, M.O. Tade, S. Wang, Coal fly ash supported Co3O4 catalysts for phenol degradation using peroxymonosulfate, RSC Advances, 2 (2012) 5645-5650.
[44] Y. Yao, Z. Yang, H. Sun, S. Wang, Hydrothermal Synthesis of Co3O4–Graphene for Heterogeneous Activation of Peroxymonosulfate for Decomposition of Phenol, Industrial & Engineering Chemistry Research, 51 (2012) 14958-14965.

[45] N.H. Trang, E. Kwon, G. Lisak, C. Hu, K.-Y. Andrew Lin, Cobalt ferrite nanoparticle-loaded nitrogen-doped carbon sponge as a magnetic 3D heterogeneous catalyst for monopersulfate-based oxidation of salicylic acid, Chemosphere, 267 (2021) 128906.
[46] Y. Bao, W.-D. Oh, T.-T. Lim, R. Wang, R.D. Webster, X. Hu, Elucidation of stoichiometric efficiency, radical generation and transformation pathway during catalytic oxidation of sulfamethoxazole via peroxymonosulfate activation, Water Research, 151 (2019) 64-74.
[47] X. Duan, C. Su, J. Miao, Y. Zhong, Z. Shao, S. Wang, H. Sun, Insights into perovskite-catalyzed peroxymonosulfate activation: Maneuverable cobalt sites for promoted evolution of sulfate radicals, Applied Catalysis B: Environmental, 220 (2018) 626-634.
[48] Q. Wang, Y. Shao, N. Gao, W. Chu, J. Chen, X. Lu, Y. Zhu, N. An, Activation of peroxymonosulfate by Al2O3-based CoFe2O4 for the degradation of sulfachloropyridazine sodium: Kinetics and mechanism, Separation and Purification Technology, 189 (2017) 176-185.
[49] W. Guo, S. Su, C. Yi, Z. Ma, Degradation of antibiotics amoxicillin by Co3O4-catalyzed peroxymonosulfate system, Environmental Progress & Sustainable Energy, 32 (2013) 193-197.
[50] A. Rastogi, S.R. Al-Abed, D.D. Dionysiou, Sulfate radical-based ferrous–peroxymonosulfate oxidative system for PCBs degradation in aqueous and sediment systems, Appl Catal B, 85 (2009) 171-179.
[51] L.J. Xu, W. Chu, L. Gan, Environmental application of graphene-based CoFe2O4 as an activator of peroxymonosulfate for the degradation of a plasticizer, Chemical Engineering Journal, 263 (2015) 435-443.
[52] P. Liang, C. Zhang, X. Duan, H. Sun, S. Liu, M.O. Tade, S. Wang, An insight into metal organic framework derived N-doped graphene for the oxidative degradation of persistent contaminants: formation mechanism and generation of singlet oxygen from peroxymonosulfate, Environmental Science: Nano, 4 (2017) 315-324.
[53] R. Luo, M. Li, C. Wang, M. Zhang, M.A. Nasir Khan, X. Sun, J. Shen, W. Han, L. Wang, J. Li, Singlet oxygen-dominated non-radical oxidation process for efficient degradation of bisphenol A under high salinity condition, Water Research, 148 (2019) 416-424.
[54] S. Yang, P. Wu, J. Liu, M. Chen, Z. Ahmed, N. Zhu, Efficient removal of bisphenol A by superoxide radical and singlet oxygen generated from peroxymonosulfate activated with Fe0-montmorillonite, Chemical Engineering Journal, 350 (2018) 484-495.

[55] L. Peng, X. Gong, X. Wang, Z. Yang, Y. Liu, In situ growth of ZIF-67 on a nickel foam as a three-dimensional heterogeneous catalyst for peroxymonosulfate activation, RSC Adv, 8 (2018) 26377-26382.
[56] R. Lan, W. Su, J. Li, Preparation and Catalytic Performance of Expanded Graphite for Oxidation of Organic Pollutant, Catalysts, 9 (2019) 280.
[57] X. Duan, K. O'Donnell, H. Sun, Y. Wang, S. Wang, Sulfur and Nitrogen Co-Doped Graphene for Metal-Free Catalytic Oxidation Reactions, Small, 11 (2015) 3036-3044.
[58] D.E. Latch, K. McNeill, Microheterogeneity of singlet oxygen distributions in irradiated humic acid solutions, Science, 311 (2006) 1743-1747.